Dual-modal Light-harvesting Microfluidic System via Simultaneous Up- and Down-Conversions for Enhanced Flow Photocatalysis

Mi-Jeong Kim
Pohang University of Science and Technology
Younghoon You
Ulsan National Institute of Science and Technology
Gwang-Noh Ahn
Pohang University of Science and Technology (POSTECH)
Sanghyeon Bae
Ulsan National Institute of Science and Technology
Dowon Kim
Ulsan National Institute of Science and Technology
Jung-Kyun Kim
Center for Scientific Instrumentation, Korea Basic Science Institute (KBSI)
Yong-Eun Kwon
Chungnam National University
Jungki Ryu
Ulsan National Institute of Science and Technology https://orcid.org/0000-0002-0897-8463
Jiseok Lee
Ulsan National Institute of Science and Technology https://orcid.org/0000-0003-2968-2458
Dong-Pyo Kim (dpkim@postech.ac.kr)
Pohang University of Science and Technology

Article

Keywords: Photocatalysis, dual-modal light-harvesting, down-conversion, upconverting nanocrystals, microfluidic system, aza-Henry reaction.

Posted Date: December 28th, 2020

DOI: https://doi.org/10.21203/rs.3.rs-124099/v1

Abstract

Microfluidic systems with large surface-to-volume ratios enable photocatalytic reactions to occur, avoiding the limitations of light penetration and allow the efficient transfer/mixing of mass and energy. For enhanced photocatalysis, the utilization of broad-spectrum light, especially over the entire solar spectrum, is highly desirable, but has been less explored in microfluidic systems. Herein, we report a novel microfluidic system with dual-modal light-harvesting capability via simultaneous up- and down-conversions to significantly improve the photocatalytic efficiency of C(sp^3)-H functionalization reactions using ultraviolet (UV) to near-infrared (NIR) light. A transparent composite incorporating down-converting (DC) coumarin dye and up-converting (UC) lanthanide-doped nanocrystals (β-$NaYF_4$:Yb/Er/Gd) was coated onto the inner surface of the microchannels, which showed effective dual conversion of UV/NIR to visible light. An improved photocatalytic organic transformation using our single- or double-stacked microfluidic system was achieved utilizing a photocatalytic aza-Henry reaction with rose bengal (RB), which displayed a two-fold increase in reaction conversion.

Introduction

Artificial photocatalysis mimics natural photosynthesis to achieve sustainable and environmentally benign chemical synthesis using light energy. In particular, photoredox catalysis using various organic photocatalysts is inexpensive and exhibits low toxicity.[1−3] However, photochemical organic transformations often occur at limited penetration distances due to the utilization of light through absorbing media. Consequently, the transformation efficiency may be low in conventional bulk reactors. Therefore, microfluidic systems with large surface-area-to-volume ratios are promising platforms to overcome such restrictions toward efficient photocatalytic organic synthesis.[4−8] This approach affords various advantages, such as short light pathway and uniform distribution of light, which lead to a noticeable decrease in reaction time and increase in the product yield or selectivity compared to those obtained using batch reactors, even under mild conditions.[9−12]

Recently, several microfluidic systems efficiently harvest light by exploiting the Stokes-shift phenomenon.[13,14] For example, a photomicroreactor used for efficient chemical oxidation reactions utilizes a down-converting luminescent solar concentrator that renders an optical guiding effect in a physical medium. However, the broad space between the flow channels causes light loss due to incomplete total internal reflection. To overcome such limitations of solid-state optical guiding systems, a three-dimensional (3D) structured dual-channel microfluidic system: one for the luminophore in solution and the other acting as a reaction channel, has been developed to transfer the light effectively from the down-converting luminophore fluid channel to the reaction channel to improve the reaction efficiency by applying a controlled channel system to obtain a homogeneous luminescent field.[15] Nevertheless, these reported works only use the down-converting phenomenon to harness ultraviolet (UV) light, which is further attenuated by the inevitable light loss in the bulky physical medium during transfer.

In these contexts, the anti-Stokes-shift luminescence phenomenon of upconverting nanocrystals (UCNs) has gained attention because it enables a dual-modal light-harvesting approach using both up- and down-converters to harness UV and near-infrared (NIR) light by expanding the wavelength range of electromagnetic radiation used to activate the photocatalyst.[16,17] In addition, NIR light generally exhibits deep light penetration in physical media. Therefore, using a matrix consisting of UCNs is a promising approach toward the construction of an effective light harvester. Moreover, for efficient light transfer to a photocatalyst with less light scattering in the medium, a compact matrix of luminescence donors can be arranged in an intimate-distance manner.

In this paper, we report a rationally devised microfluidic system whose inner channel surface was coated with a thin and transparent composite comprised of up- and down-converters for dual-modal light-harvesting. This arrangement significantly increases the photocatalytic efficiency of C(sp^3)-H functionalization reactions. Coumarin 153 (C153) acting as the down-converting (DC) component and $NaYF_4$:Yb/Er/Gd nanocrystals as the up-converting (UC) component were homogeneously embedded on the surface layer of an elaborate serpentine microchannel, exhibiting high transparency (Fig. 1). The dual-modal light-harvesting behavior was confirmed using photoluminescence (PL) and photoelectrochemical (PEC) analyses under various conditions. The photocatalytic reaction of rose bengal (RB) in a single or double-stacked microfluidic system was remarkably promoted by doubling the conversion of 2-phenyl-1,2,3,4-tetrahydroisoquinoline within a short retention time (28 min) at room temperature. This result, even with a short reaction time, is the best conversion rate obtained for aza-Henry reaction with RB or other organic photocatalysts reported to date (Supplementary Table 1). Our dual-modal light-harvesting microfluidic system is a pioneering robust methodology, which can effectively enhance photoredox catalytic performance.

Results And Discussion

For efficient harvesting of a broad spectrum of light, we chose two types of highly emissive materials (Fig. 2a). Coumarin 153 (C153) is conventionally used in OLED applications, which showss superior absorption and emission properties.[18,19] C153 is completely soluble in a photocurable silane-based inorganic polymer, allylhydridopolycarbosilane (AHPCS), which exhibits high chemical resistance,[20,21] and triallyl(phenyl)silane (TAPS), which acts as a cross-linker, without phase separation. To realize dual-modal light-converting phenomena, we prepared visible light emissive lanthanide-doped UCNs (β-$NaYF_4$:Yb/Er/Gd; 30/2/30 mol%) using a conventional hydrothermal method (Fig. 2a; the detailed synthetic method is described in the Supplementary Information). The unique up-converting luminescence characteristics of UCNs have been studied in various fields, including photovoltaics, encoding, bioimaging, and drug delivery.[22–29] Upon exposure to 980-nm NIR light, the synthesized UCNs showed luminescence at 530 and 660 nm, which overlaps with the absorption spectra of RB in the wavelength range 520–550 nm. The UCNs were capped with oleic acid (OA), which has a long hydrocarbon chain, to form a well-dispersed mixture in the hydrophobic AHPCS/TAPS matrix. Notably, the emission ranges of C153 and the UCNs are complementary to the absorption range of RB

(Supplementary Fig. 1), which were elaborately used for dual-modal light-harvesting via simultaneous up- and down-conversions.

A thin-film sample was first manufactured using a polymeric mixture dispersed with C153 and UCNs using free radical polymerization to confirm their homogeneous dispersion in the solid-state composite. The FT-IR spectra (Fig. 2b) of the consolidated composite film showed that the photo- and thermal-curing process eliminates the C = C bonds (1620–1630 cm^{-1}) originating from the OA in the UCNs and the AHPCS/TAPS pre-polymer. Accordingly, the OA-capped UCNs were covalently cross-linked with the silane-based polymer matrix via C–C bonding and uniformly distributed in the solid-state composite. We also investigated the transmittance of the composite film on the PDMS substrate in the absorption range of RB using UV-Vis spectroscopy (Fig. 2c). A thin composite film with a thickness of ~ 40 *μm* was then manufactured using the optimized content of C153 (1 wt.%) and UCNs (8 wt.%). The high transparency of the film indicates the uniform distribution of C153 and UCNs without phase separation. The bare PDMS substrate has ~ 90% transparency in the UV, Vis, and NIR light region. The composite film on the substrate exhibits the remarkable absorption of C153 at < 450 nm, presenting a slightly yellow tint by absorbing UV light (Fig. 2c; see inset photograph). In addition, the high transmittance of ~ 80% in the wavelength range 450–600 nm allows sufficient transfer of visible light to enable RB photocatalysis in the microfluidic channels even after coating with the composite.

We fabricated a composite-coated microfluidic system (Fig. 3a) to perform enhanced photocatalytic reactions by harvesting a broader spectrum of light. To replicate the polydimethylsiloxane (PDMS) microchannels, two molds with different cross-sectional dimensions (~ 1000 *μm* × 1000 *μm* vs. ~500 *μm* × 500 *μm*) and total lengths (33 cm vs. 132 cm) were made, which were manufactured using a 3D printer (Supplementary Fig. 2). The inner surface of the PDMS microchannels was coated with a thin layer of the composite resin after a serial procedure consisting of partial UV curing, removal of the filled resin with air-blowing, and post-thermal curing steps. The microfluidic systems with luminescence donors were successfully prepared with inner volumes of ~ 280 and ~ 215 *μ*L, respectively. The detailed morphology of the fabricated microchannels was investigated by cutting the microchannel in both transverse and horizontal cross-sections, followed by SEM analysis (Fig. 3). The cross-section of the microchannel was slightly different from the square shape, presumably due to the low resolution of the 3D printed molds. From the SEM images, we can see that the thicknesses of the composite on the channel surfaces roughly varied with lengths in the range from several micrometers to ~ 40 *μm*. In addition, energy dispersive X-ray spectroscopy (EDS) mapping was performed using the horizontally cut samples to further examine the distribution of the UCNs (Fig. 3e). The uniform presence of Na, Gd, Yb, Er, and Y in the microchannels indicates the homogeneous dispersion of the UCNs in the coating of the microchannels. These results consistently suggest the uniform dispersion of the UCNs on the microchannels was achieved after the fabrication process.

The luminescence properties of the fabricated composite film and microfluidic systems were confirmed using fluorescence microscopy and the naked eye under UV (405 nm) and NIR (980 nm) light. Photographs of the optical luminescence indicate that the luminescence donors (C153 and UCNs) were

well-distributed throughout the entire microchannel pattern (~ 1000 *μm* channel width) (Fig. 4a, left and Fig. 4b, left). A similar aspect of luminescence was observed in a more complex serpentine microchannel pattern (~ 500 *μm* channel width) (Supplementary Fig. 3). Moreover, we confirmed that the emitted visible light was quenched by RB dissolved in a mixed solution of acetonitrile, nitromethane, and deionized water under both UV and NIR light (Fig. 4a, right and Fig. 4b, right). The photoluminescence (PL) spectra were measured to further verify the light-converting phenomena (Fig. 4c, dark grey line and Fig. 4d, dark grey line). The PL spectra of the consolidated composite matrix showed that C153, which exhibited a maximum absorption wavelength (λ_{max}) at 400 nm and a minimum absorption wavelength (λ_{edge}) at 470 nm (Fig. 2b, blue line), emitted a luminescence λ_{max} at 470 nm and λ_{edge} at 580 nm (Fig. 4c). Hence, the luminescence emitted from C153 in the wavelength range 480–590 nm disappeared in the presence of RB in the microchannels. Characteristic luminescence peaks of the UCNs were observed at 520 and 550 nm when excited using 980-nm NIR light (Fig. 4d). The luminescence intensity of the UCNs in the visible light region also decreased in the presence of RB in the microchannels. That is, the luminescence of both C153 and UCNs was considerably quenched by absorption in the RB solution (Supplementary Fig. 1), confirming the dual-modal light transfer from C153 and the UCNs to RB, respectively.

We further performed photoelectrochemical (PEC) analysis to confirm the harvesting of up- and down-converted light from the composite film by RB. PEC analysis was conducted using RB-coated TiO_2 nanotubes (NTs) as the working electrode (Supplementary Fig. 6a). White and/or NIR light was irradiated on the working electrode through a glass slide with and without the composite film layer (Fig. 4e and Supplementary Fig. 6b). Significantly increased photocurrent densities were measured at 1.36 V only when the light was irradiated through the composite film for both white and NIR light. On the contrary, no or a negligible enhancement was observed when the bare glass slide was employed (Fig. 4e). Considering that the photocurrent can be induced when the adsorbed RB generates and injects photoexcited electrons into the TiO_2 NTs, these results demonstrate (1) the successful conversion of white and NIR light (i.e., dual conversion) to visible light by the composite film and (2) the harvesting of the converted light by RB for photocatalysis.

Table 1. Photocatalytic aza-Henry reaction conducted using various light sources and luminescence donors in the dual-modal light-harvesting microfluidic system prepared with the coated composite.[a]

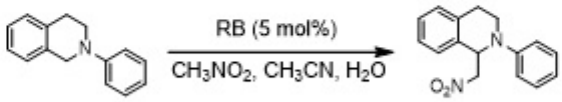

Entry	Content of Composite	Light	Conversion (%)[b]
1	None	UV + Vis + NIR	42
2	C153 1 wt.% + UCNs 4 wt.%	UV + Vis + NIR	57
3	C153 1 wt.% + UCNs 8 wt.%	UV + Vis + NIR	74
4	C153 1 wt.% + UCNs 8 wt.%	UV	33
5	C153 1 wt.% + UCNs 8 wt.%	NIR	14
6	C153 1 wt.% + UCNs 8 wt.%	UV + Vis	45
7	None*	UV + Vis + NIR	67
8	C153 1 wt.% + UCNs 8 wt.%*	UV + Vis + NIR	97

[a] The reactions were conducted using 2-phenyl-1,2,3,4-tetrahydroisoquinoline (0.075 M) in a $CH_3CN/CH_3NO_2/H_2O$ (1:0.8:0.2 ratio) solution under UV, Vis, or NIR light at a flow rate of 10 μL min^{-1} and 7.5 μL min^{-1}* in two microfluidic systems (channel width: ~1000 μm and ~500 μm*). Retention time = 28 min. [b] The conversion was determined using ^{1}H NMR spectroscopy.

We calculated the light penetration depth of the RB solution using the Beer–Lambert law ($A = \varepsilon cl = -\log T$; where A = absorbance, ε = molar absorption coefficient, c = concentration, l = path length, and T = transmittance)[11] to determine how much light can pass through the solution. The calculated plot showed that light transmittance dropped exponentially with the light penetration depth (Supplementary Fig. 8). RB with an absorption coefficient of 26,819 M^{-1} cm^{-1} at λ_{max} = 559 nm (Supplementary Fig. 1), may allow very little light to penetrate (< 0.5% at l = 250 μm) to the inside of the RB solution in acetonitrile, nitromethane, and deionized water in the microfluidic channels. Therefore, this estimation suggests the use of a microfluidic system with a shorter channel width (~ 500 μm) to further improve the organic transformation performance. The conversion in the channel without the up- and down-converters was 67%, which was higher than the 42% conversion obtained in the longer microchannel (~ 1,000 μm) at the

same retention time (Table 1; entries 1 and 7). It was confirmed that the presumed light pathlength of 250 *μm* was favorable for superior photoredox catalysis with a channel width of ~ 500 *μm*.

Eventually, the use of a microfluidic system with a smaller channel width (~ 500 *μm*) coated with a composite containing UC and DC components showed a significantly improved conversion of 97% under dual-modal light harvesting conditions (Table 1 and Supplementary Fig. 9). To the best of our knowledge, this is the highest conversion versus reaction time obtained for the aza-Henry reaction using RB or other organic photocatalysts (Supplementary Table 1). This result was achieved due to the synergistic advantages of simultaneous up- and down-converting phenomena combined with the microfluidic system with effective light penetration and high surface-area-to-volume ratio (Supplementary Fig. 3).

The increase in the production capacity using microreactors has been considered without loss of reaction efficiency.[30,31] The dual-modal light-harvesting methodology of microfluidic systems was has been attempted in a similar manner by linearly stacking the composite-coated microfluidic system (Fig. 4). The second layered channel plate was tilted 15° over the first layered plate to minimize the overlapped channels for effective light delivery (Supplementary Fig. 10). This double-stacked system increases the reaction volume (~ 430 *μ*L) and flow rate as much as two-fold in terms of the productivity. The aza-Henry reaction in the double-stacked system showed an identical conversion of 97% for a retention time of 28 min when compared to the result in the single devices. Moreover, the C–C coupling reactions of nitromethane and diethyl malonate gave product **b** with 99% conversion and C–P bond formation of the diethyl phosphite gave the corresponding product (**c**) with 63% conversion at a retention time of 28 min. These results show not only the superior photocatalytic efficiency, but also the increased production capacity of our stacked-up system manufactured using the UC and DC components.

Conclusions

In summary, we successfully developed a novel dual-modal light-harvesting microfluidic system by coating a transparent composite resin incorporated with C153 dye as the DC component and lanthanide-doped nanocrystals ($NaYF_4$:Yb/Er/Gd) as the UC component. The manufactured AHPCS/TAPS based composite film encapsulating C153 and the UCNs maintained excellent luminescence properties when irradiated with both UV and NIR light with high transparency (~ 80%) in the visible light region. The emitted light from the composite matrix was quenched in the presence of RB. The improved electron excitation of RB was also confirmed by observing the higher photocurrent density when white and NIR light was used to irradiate the composite film on a glass substrate when compared to the bare glass substrate. Moreover, the serpentine microfluidic systems fabricated with the chosen composite showed visible light emission from the DC and UC components, and considerable luminescence quenching in the presence of RB. Based on the Beer–Lambert law, we obtained the highest conversion (97%) in the microsystem containing the DC and UC components with a narrow channel width (~ 500 *μm*) when conducting the photocatalytic aza-Henry reaction. This result is superior to the 42% conversion obtained in the wider system (~ 1000 *μm*) without the DC and UC components under identical light sources and a retention time of 28 min. Moreover, the double-stacked microsystem retained its excellent conversion of

97% with increased productivity. It is believed that rationally designed transparent up- and down-converting matrices on the microfluidic channels is a promising approach for light-harvesting to attain effective photocatalysis for sustainable chemistry.

Methods

General Information

Polydimethylsiloxane (PDMS, Sylgard 184) and the curing agent (Sylgard 184) were purchased from Dow Corning. Allylhydridopolycarbosilane (AHPCS, $[Si(CH_2CHCH_2)_2CH_2]_x[SiH_2CH_2]_{n-x}$, x = 0.5%, SMP-10) as an organic-inorganic hybrid oligomer (Mw 450 Da; viscosity, 0.1 Pas; color light, yellow) was purchased from Starfire System. Irgacure369 was purchased from Ciba Specialty Chemicals. UCNs were synthesized (Supplementary Information) using oleic acid (technical grade, 90%), $GdCl_3•6H_2O$ (99.9%), $YCl_3•6H_2O$ (99.9%), $YbCl_3•6H_2O$ (99.9%), $ErCl_3•6H_2O$ (99.9%), and NH_4F (99.9%), which were purchased from Sigma-Aldrich. NaOH was purchased from Daejung. The starting material for the aza-Henry reaction was synthesized (Supporting Information). All other reagents were purchased from Merck (Sigma-Aldrich), Tokyo Chemical Industry Co. Korea (TCI Korea) or Samchun Chemicals Polytetrafluoroethylene (PTFE) tubing (i.d. = 1 mm, o.d. = 1/16") was purchased from IDEX HEALTH & SCIENCE (WA, USA).

Fabrication Of Dual-modal Light-harvesting Microfluidic Systems With Composite Resin

The PDMS microfluidic channel was prepared by replicating the polymer molds manufactured using a multi-jet printing (MJP) 3D printer (ProJet-MJP 3600). The 3D printed molds with the designed microchannel patterns were commissioned to K-TECH Co. Ltd in Korea (Supplementary Fig. 2). The mixed viscous precursor of PDMS at a ratio of 10:1 was poured onto the 3D-printed mold and then cured at 80 °C for 2 h. After soft lithography, the PDMS and patterned PDMS substrates were treated with O_2 plasma for 2 min at 70 W and then bonded to each other to form the microchannels. The inlet and outlet tubing were connected to the PTFE tubing. Both C153 and UCNs were premixed at various ratios of 1:4–8 wt.% in the AHPCS/TAPS polymer resin with a photo-curing agent (irgacure369, 2 wt.%) and thermal curing agent (dicumyl peroxide, 2 wt.%). The mixer resin was introduced into the microfluidic channel via PTFE tubing. The fully filled microfluidic devices were exposed to a Xe lamp (300 W) for 3 min to homogeneously coat the inner channel surface and the uncured resin in the channel was removed and washed with isopropanol. The partially cured composite resin on the microfluidic channel surface was completely consolidated upon post-thermal curing in an oven at 80 °C overnight.

Characterization Of The Composite Film And Composite Coated Microchannels

Fourier-transform infrared spectroscopy (FT-IR) spectra were obtained on a Jasco FT/IR-4600 spectrometer using KBr pellets for the raw materials or neat using ATR accessories for the consolidated composite film on the PDMS substrate. Scanning electron microscopy (SEM) images were obtained using a field-emission scanning electron microscope (FE-SEM, Merlin, Carl Zeiss or JSM-7800F Prime, JEOL Ltd.) operated at 0.02–30 kV. To confirm the uniform distribution of C153 and UCNs in the

composite-coated microchannel, electron dispersion spectroscopy (EDS) mapping and elemental analysis were performed using an EDS detector (XFlash 6l60, Bruker: Take-off angle, 35°; detector area, 60 mm^3 or Quad Detector (LED,UED,USD,BED) and EDS analysis software (ESPRIT 2.0.0, Bruker or Aztec, Oxford Instruments).

Analysis Of Dual-modal Light-harvesting Performance

The absorption properties of the RB solution (3.5 μM) and the composite film were measured using a UV-Vis spectrometer (NANODROP 2000c, Thermo Scientific) in a 10-mm quartz cuvette for the solution-state and a double-beam Shimadzu UV-2550 spectrophotometer over 300–800 nm for the solid-state film. The luminescence properties of the composite films and the solutions were measured using a PL spectrofluorometer (FP-6500, JASCO). In addition, the PL spectra of the microfluidic channels fabricated with the composite film were measured using a self-designed spectrometer (QE Pro, Ocean Optics) containing a 980-nm continuous wave (CW) laser source (Dragon Lasers, China). A 980-nm CW laser (40 W, Changchun New Industries Optoelectronics Tech. Co. Ltd., China) was used as a NIR light source. The photocurrent of the composite resin was measured using chronoamperometry (CA) in three-electrode PEC cells composed of TiO_2 nanotubes (NTs) as the working electrode, fluorine-doped tin oxide (FTO) coated Pt as the counter electrode, and Ag/AgCl as the reference electrode. The PEC test was conducted in 0.2 M Na_2SO_4 (aq) electrolyte (pH 7) with the composite-coated glass and bare glass substrates under a 27 W white LED source or 40 W NIR laser source. For the CA measurements, RB was dissolved in the electrolyte (0.2 M) and TiO_2 NTs modified with the RB catalysts were fabricated by drop-casting method using a 2.5 M RB solution. The potentials were regulated using an SP-150 potentiostat (Bio-Logic Science Instruments, France) at 1.36 V vs RHE.

Continuous-flow Photocatalysis of C(sp^3)-H Functionalization Reactions

Photocatalytic flow reactions were performed under a blue LED (11 W, 9 × 10 cm^2, λ_{max} = 405 nm) as the UV light source, white LED (27 W, 11 × 15 cm^2, 8000 K) as the UV and Vis light source, and a 980-nm CW laser (Dragon Lasers, China) or 980-nm CW laser (40 W, Changchun New Industries Optoelectronics Tech. Co. Ltd., China) as an NIR light source. The solution of starting reagent (0.075 M) mixed with RB (5 mol%) in acetonitrile, reactant, and H_2O (1:0.8:0.2 v/v/v) was fed into the fabricated microfluidic devices using a KD Scientific Legato 180 syringe pump (Holliston, MA, USA). ^1H NMR (300, 400, or 500 MHz) and ^{13}C NMR (125 MHz) spectra were recorded on a Bruker AVANCE III HD 300, 400 or 500-MHz NMR spectrometer in $CDCl_3$.

Declarations

Acknowledgements

This study was supported by the National Research Foundation (NRF) of Korea grants funded by the Korean government (MSIT) (NRF-2017R1A3B1023598 and NRF-2018R1D1A1A02046918) and the

Institute of Civil Military Technology Cooperation Center (ICMTC) funded by the Ministry of Trade, Industry and Energy, and Defense Acquisition Program Administration of Korea (18-CM-SS-13).

References

1. Zhang, W. et al. Direct C–H difluoromethylation of heterocycles via organic photoredox catalysis. *Nat. Commun.* **11,** 1–10 (2020).
2. Zhang, Y., Schilling, W., Riemer, D. & Das, S. Metal-free photocatalysts for the oxidation of non-activated alcohols and the oxygenation of tertiary amines performed in air or oxygen. *Nat. Protoc.* **15,** 822–839 (2020).
3. Schilling, W., Riemer, D., Zhang, Y., Hatami, N. & Das, S. Metal-free catalyst for visible-light-induced oxidation of unactivated alcohols using air/oxygen as an oxidant. *ACS Catal.* **8,** 5425–5430 (2018).
4. Laudadio, G. *et al.* C(sp^3)-H functionalizations of light hydrocarbons using decatungstate photocatalysis in flow. *Science* **369,** 92–96 (2020).
5. Seo, H., Katcher, M. H. & Jamison, T. F. Photoredox activation of carbon dioxide for amino acid synthesis in continuous flow. *Nat. Chem.* **9,** 453–456 (2017).
6. Seo, H., Liu, A. & Jamison, T. F. Direct β-selective hydrocarboxylation of styrenes with CO_2 enabled by continuous flow photoredox catalysis. *J. Am. Chem. Soc.* **139,** 13969–13972 (2017).
7. Staveness, D., Collins, J. L., McAtee, R. C. & Stephenson, C. R. J. Exploiting imine photochemistry for masked N-centered radical reactivity. *Angew. Chem. Int. Ed.* **58,** 19000–19006 (2019).
8. Magallanes, G. et al. Selective C-O bond cleavage of lignin systems and polymers enabled by sequential palladium-catalyzed aerobic oxidation and visible-light photoredox catalysis. *ACS Catal.* **9,** 2252–2260 (2019).
9. Cambié, D., Bottecchia, C., Straathof, N. J. W., Hessel, V. & Noël, T. Applications of continuous-flow photochemistry in organic synthesis, material science, and water treatment. *Chem. Rev.* **116,** 10276–10341 (2016).
10. Rehm, T. H. reactor technology concepts for flow photochemistry. *ChemPhotoChem* **4,** 235–254 (2019).
11. Sambiagio, C. & Noël, T. flow photochemistry: shine some light on those tubes! *Trends Chem.* **2,** 92–106 (2020).
12. Jang, S., Jung, B. J., Kim, M. J., Lee, W. & Kim, D. P. Reaction-volume dependent chemistry of highly selective photocatalytic reduction of nitrobenzene. *React. Chem. Eng.* **4,** 1752–1756 (2019).
13. Cambié, D., Zhao, F., Hessel, V., Debije, M. G. & Noël, T. A leaf-inspired luminescent solar concentrator for energy-efficient continuous-flow photochemistry. *Angew. Chem. Int. Ed.* **56,** 1050–1054 (2017).
14. Cambié, D. et al. Energy-efficient solar photochemistry with luminescent solar concentrator based photomicroreactors. *Angew. Chem. Int. Ed.* **58,** 14374–14378 (2019).
15. Zhang, L. *et al.* Fluorescent fluid in 3D-printed microreactors for the acceleration of photocatalytic reactions. *Adv. Sci.* **6,** 1–6 (2019).

16. Wen, S. *et al.* Advances in highly doped up-conversion nanoparticles. *Nat. Commun.* **9,** 1–11 (2018).
17. Baek, D. *et al.* Multi-color luminescence transition of up-conversion nanocrystals via crystal phase control with SiO_2 for high temperature thermal labels. *Adv. Sci.* **7,** 1–9 (2020).
18. Matsushima, T. *et al.* Enhanced electroluminescence from organic light-emitting diodes with an organic–inorganic perovskite host layer. *Adv. Mater.* **30,** 1–7 (2018).
19. Gutiérrez, M., Sánchez, F. & Douhal, A. Efficient multicolor and white light emission from Zr-based MOF composites: Spectral and dynamic properties. *J. Mater. Chem. C* **3,** 11300–11310 (2015).
20. Ko, D. H. et al. Superamphiphobic silicon-nanowire-embedded microsystem and in-contact flow performance of gas and liquid streams. *ACS Nano* **10,** 1156–1162 (2016).
21. Vishwakarma, N. K., Hwang, Y. H., Adiyala, P. R. & Kim, D. P. Flow-assisted switchable catalysis of metal ions in a microenvelope system embedded with core-shell polymers. *ACS Appl. Mater. Interfaces* **10,** 43104–43111 (2018).
22. Li, Y. *et al.* Synergic effects of up-conversion nanoparticles $NaYbF_4$:Ho^{3+} and ZrO_2 enhanced the efficiency in hole-conductor-free perovskite solar cells. *Nanoscale* **10,** 22003–22011 (2018).
23. Kakavelakis, G., Petridis, K. & Kymakis, E. Recent advances in plasmonic metal and rare-earth-element up-conversion nanoparticle doped perovskite solar cells. *J. Mater. Chem. A* **5,** 21604–21624 (2017).
24. Lee, J. *et al.* Ultra-wideband multi-dye-sensitized upconverting nanoparticles for information security application. *Adv. Mater.* **29,** 1–7 (2017).
25. Kwon, O. S. *et al.* Dual-color emissive up-conversion nanocapsules for differential cancer bioimaging in vivo. *ACS Nano* **10,** 1512–1521 (2016).
26. Gu, B. & Zhang, Q. Recent advances on functionalized upconversion nanoparticles for detection of small molecules and ions in biosystems. *Adv. Sci.* **5,** 170069 (2018).
27. Lee, J. *et al.* Universal process-inert encoding architecture for polymer microparticles. *Nat. Mater.* **13,** 524–529 (2014).
28. Jalani, G. *et al.* Photocleavable hydrogel-coated upconverting nanoparticles: A multifunctional theranostic platform for NIR imaging and on-demand macromolecular delivery. *J. Am. Chem. Soc.* **138,** 1078–1083 (2016).
29. Baek, D. *et al.* Multi-color luminescence transition of upconversion nanocrystals via crystal phase control with SiO_2 for high temperature thermal labels. *Adv. Sci.* **7**, 1–9 (2020).
30. Yim, S. J. *et al.* Compact reaction-module on a pad for scalable flow-production of organophosphates as drug scaffolds. *Lab Chip* **20**, 973–978 (2020).
31. Zhao, F. *et al.* Scale-up of a luminescent solar concentrator-based photomicroreactor via numbering-up. *ACS Sustain. Chem. Eng.* **6**, 422–429 (2018).

Figures

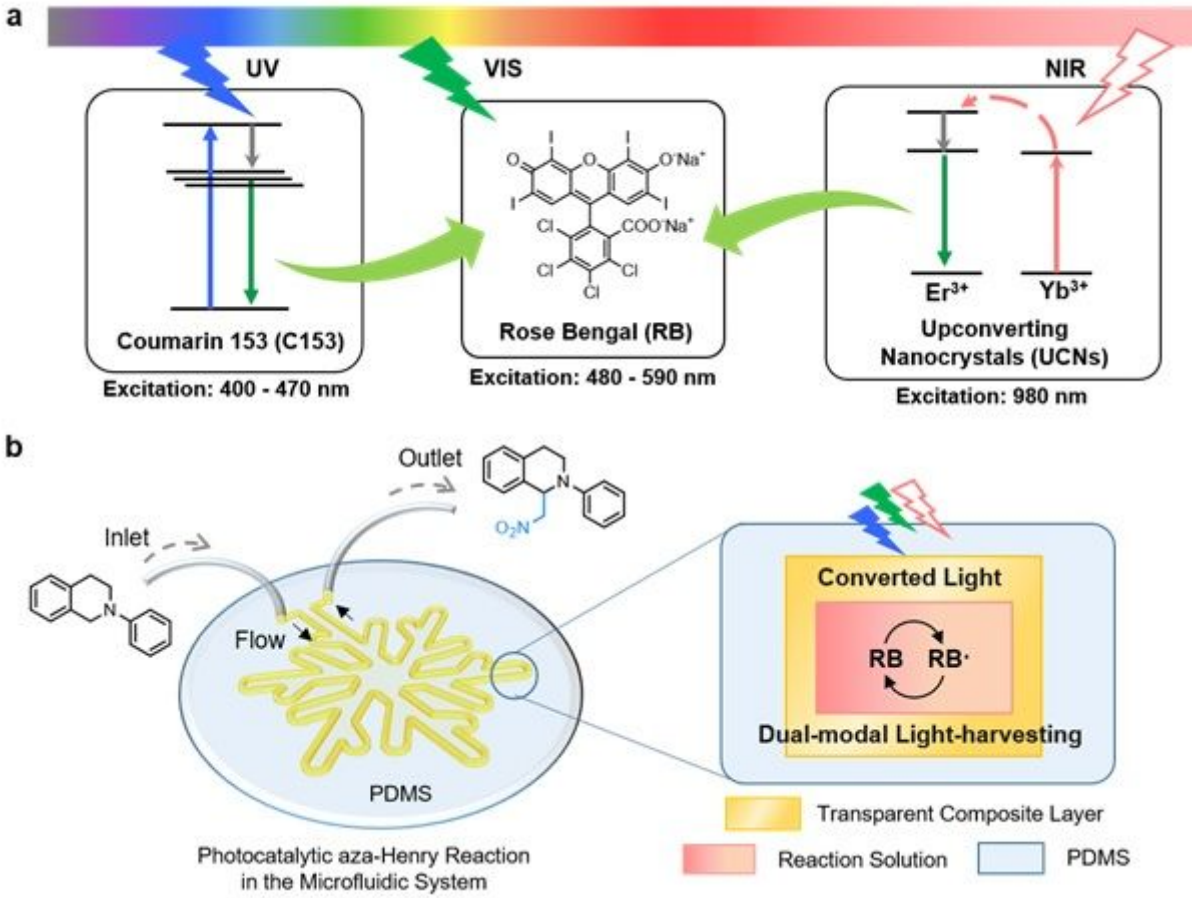

Figure 1

Schematics of (a) the dual-modal light-harvesting concept using Coumarin 153 (C153) as a down-conversion dye and NaYF4:Yb/Er/Gd as upconverting nanocrystals (UCNs) and (b) the microfluidic system with inner wall channels coated using a transparent composite resin composed of two luminescence donors used for the photocatalytic aza-Henry reaction and improved photon generation of rose bengal (RB) in the microchannels.

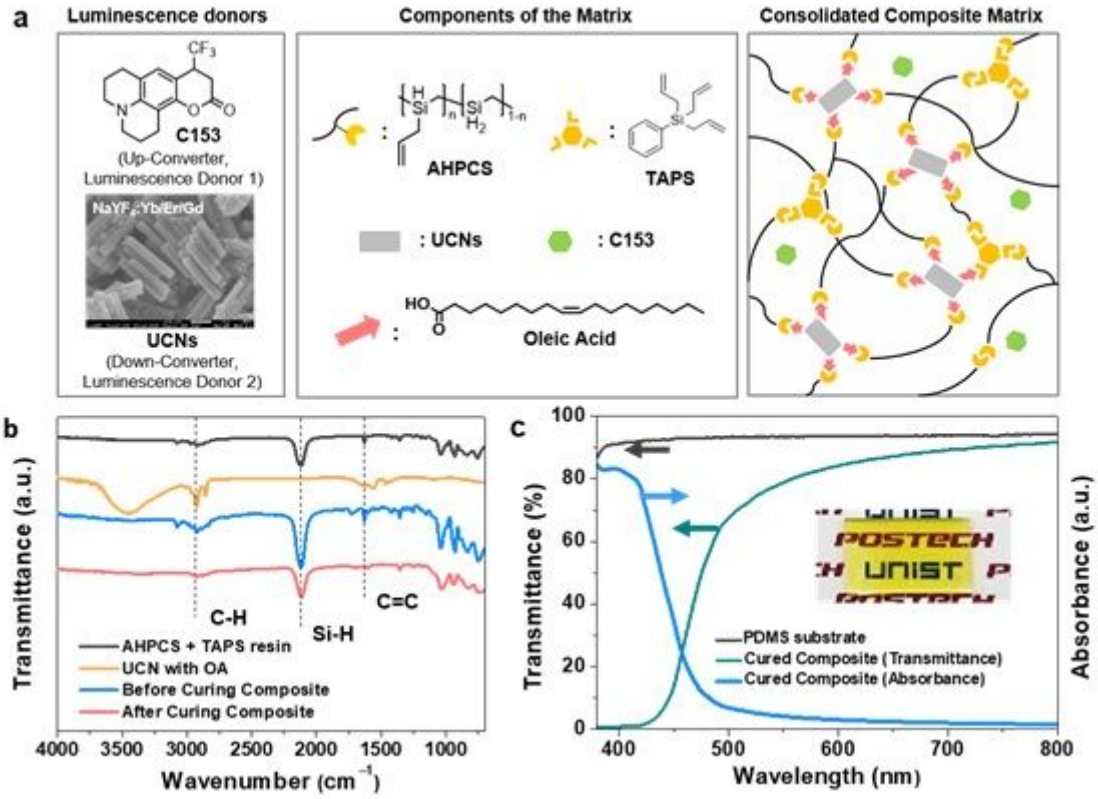

Figure 2

(a) Chemistry of UV curable composite resin as a dual-modal light harvester by embedding C153 and UCNs into an inorganic AHPCS/TAPS polymer matrix. (b) FT-IR spectra used to monitor the consolidation of the composite resin. (c) UV-Vis spectra obtained for the bare PDMS film and composite film containing C153 (1 wt.%) and UCNs (8 wt.%) on the PDMS substrate (thickness of the composite film, ~40 μm; see inset photograph).

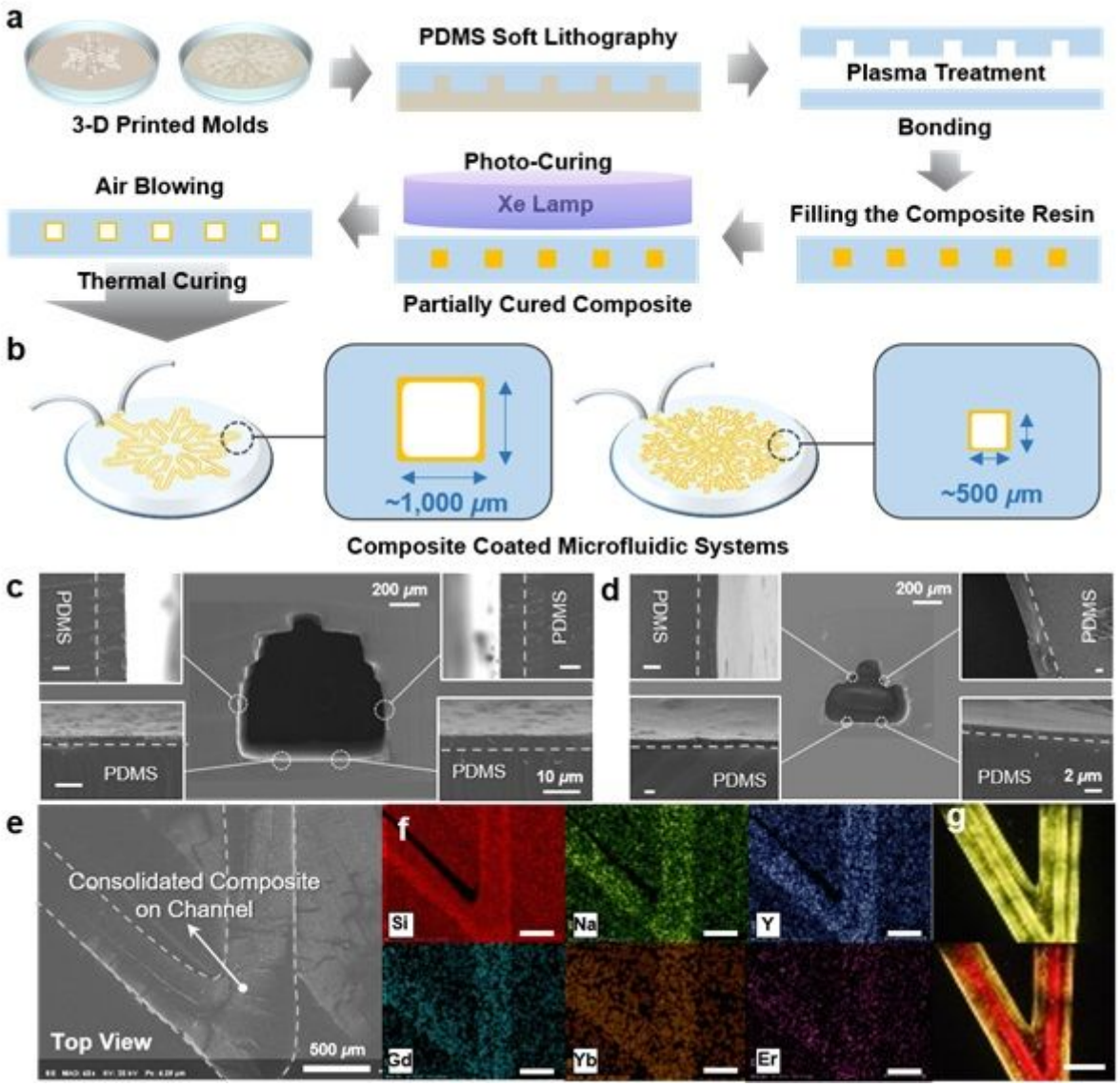

Figure 3

Schematics of (a) the fabrication of microfluidic systems by replicating the 3D printed mold with PDMS and coating the composite on the inner channel wall, (b) two types of microfluidic systems with different dimensions in terms of the cross-section and total length of the serpentine microchannels: ~1000 μm × 1000 μm area and 33 cm length on circular plate (5 cm diameter); ~500 μm × 500 μm area and 132 cm length on the circular plate (6 cm diameter). The SEM images shown in (c) and (d) are the cross-sections of the composite coated microchannels. (e) Top-view image of the microchannel (~500 μm × 500 μm) horizontally cut at the corner. (f) EDS elemental mapping of the part shown in (e) for Si, Na, Y, Gd, Yb, and Er. (g) Optical fluorescence microscopy images under NIR light of the microchannel filled with acetonitrile (top) and the RB solution (bottom).

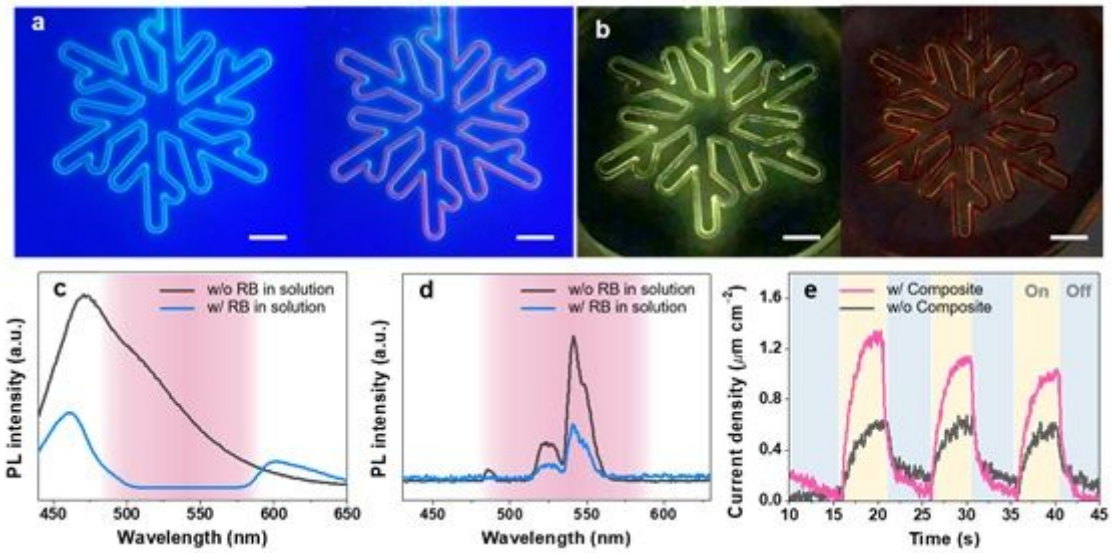

Figure 4

Photographs of the microfluidic systems filled with acetonitrile (left) and RB dissolved in a mixed solution of acetonitrile, nitromethane, and H2O (right) under (a) UV (405 nm) and (b) NIR (980 nm) light (Scale bar, 5 mm). The PL spectra of (c) the composite films at an excitation wavelength of 405 nm and (d) the composite coated channel (1,000 μm) at 980 nm with and without RB. (e) The photocurrent density measured with the composite film (pink line) on glass under on/off conditions of white and NIR light compared to the bare glass substrate with no composite film (dark grey line).

Supplementary Files

This is a list of supplementary files associated with this preprint. Click to download.

- ESIPhotocatalysisUCN.docx